ANALYSIS OF TIME-RESOLVED FLUORESCENCE ANISOTROPY DECAYS

ALBERT J. CROSS AND GRAHAM R. FLEMING
Department of Chemistry and The James Franck Institute, The University of Chicago, Chicago, Illinois 60637

ABSTRACT We discuss the analysis of time-correlated single photon counting measurements of fluorescence anisotropy. Particular attention was paid to the statistical properties of the data. The methods used previously to analyze these experiments were examined and a new method was proposed in which parallel- and perpendicular-polarized fluorescence curves were fit simultaneously. The new method takes full advantage of the statistical properties of the measured curves; and, in some cases, it is shown to be more sensitive than other methods to systematic errors present in the data. Examples were presented using experimental and simulated data. The influence of fitting range on extracted parameters and statistical criteria for evaluating the quality of fits are also discussed.

INTRODUCTION

Time-resolved fluorescence depolarization on the nanosecond and sub-nanosecond time scales is a powerful technique for the study of rapid motions of molecules in liquids (1–5). Information about the microscopic motions is contained in the time-dependent emission anisotropy, $r(t)$, which can be related to a correlation function of the transition moment in the laboratory frame (6–9). If the transition dipoles for absorption of the excitation and emission of fluorescence are $\underset{\sim}{\mu}_a$ and $\underset{\sim}{\mu}_e$, respectively, the emission anisotropy is given by

$$r(t) = \tfrac{2}{5} \langle P_2 [\underset{\sim}{\mu}_a(0) \cdot \underset{\sim}{\mu}_e(t)] \rangle, \quad (1)$$

where $P_2(x)$ is the second legendre polynomial and the angle brackets denote ensemble average. Thus the time-resolved anisotropy provides a direct probe of molecular motion and other relaxation processes.

Over the past decade, the method of time-correlated single photon counting has been used to obtain time-resolved polarized fluorescence data in several laboratories (10–29). Other methods were used to obtain these data, including up-conversion (30) and recording intensity profiles with a streak camera (31), but the photon-counting technique has the advantages of the large dynamic range, which can be attained (typically four or five decades or more), and the well-understood statistical properties, which apply to the data (32).

There are two features of fluorescence anisotropy experiments that cause complications in their analysis. First, the anisotropy cannot be directly measured; it must be extracted from the observed polarized emission curves, $I_\parallel(t)$ and $I_\perp(t)$. In addition, the familiar problem of convolution due to a system response function of finite duration causes distortions of the measured curves (33). The usual assumption made is that the apparatus acts as a linear system, so that the observed polarized emission curves are related to the true decay functions, $i_\parallel(t)$ and $i_\perp(t)$, by convolution with the instrument impulse response function, $g(t)$

$$I_\parallel(t) = \int_0^t g(t - \tau) i_\parallel(\tau) d\tau \quad (2)$$

$$I_\perp(t) = \int_0^t g(t - \tau) i_\perp(\tau) d\tau. \quad (3)$$

The excited state decay law (i.e., the concentration of molecules in the excited state), $K(t)$, and the anisotropy decay law, $r(t)$, are directly related to the nondistorted emission curves, according to relations given by Tao (6)

$$i_\parallel(t) = \tfrac{1}{3} K(t) [1 + 2r(t)] \quad (4)$$

$$i_\perp(t) = \tfrac{1}{3} K(t) [1 - r(t)]. \quad (5)$$

Or equivalently

$$K(t) = i_\parallel(t) + 2i_\perp(t) \quad (6)$$

$$r(t) = \frac{i_\parallel(t) - i_\perp(t)}{i_\parallel(t) + 2i_\perp(t)}. \quad (7)$$

Almost all methods used to obtain the time-dependent anisotropy have begun with calculating sum and difference curves from the experimental data, given by

$$S(t) = I_\parallel(t) + 2\alpha I_\perp(t) \quad (8)$$

$$D(t) = I_\parallel(t) - \alpha I_\perp(t). \quad (9)$$

Here α is a scaling factor that accounts for fluctuations in

Dr. Fleming is a Alfred P. Sloan Foundation Fellow and Camille and Henry Dreyfus Teacher Scholar.

excitation pulse intensity and variations in the conditions for collecting $I_\parallel$ and $I_\perp$, including differences in accumulation times, geometrical factors, polarization dependence of the photomultiplier tube (PMT), detection efficiency, etc. In the absence of such deviations, α is unity. In this work, we review the methods used for controlling and estimating the value of α and suggest tests that should be used to estimate errors introduced by them.

The inherent errors in the measured curves due to counting statistics are compounded in constructing $D(t)$. This results in a function for which Poisson statistics do not apply. Although error propagation can be used to calculate estimates of the variances for each channel in $D(t)$ (14, 34, 35), note that these variances are larger than those for Poisson statistics. This is because in a given channel, for the parallel or perpendicular curve, the raw data (i.e., number of counts) differs from the underlying parent value by an unknown amount, and thus gives only an imperfect estimate of that parent value. If $r(t)$ approaches zero, the counting errors in the parallel and perpendicular curves become equal or larger than the difference between them, and the calculated difference of two such estimates can be a poor approximation for the difference of the parent values.

In the absence of time shift or normalization errors, the functions $S(t)$ and $D(t)$ are the convolutions of $K(t)$ and the product $r(t)K(t)$, respectively. So, we define the lower case counterparts as the nonconvoluted functions

$$s(t) = i_\parallel(t) + 2\alpha i_\perp(t) \tag{10}$$

$$d(t) = i_\parallel(t) - \alpha i_\perp(t). \tag{11}$$

From the ratio of the functions $D(t)$ and $S(t)$, the point-by-point anisotropy, $R(t)$, can be constructed

$$R(t) = \frac{D(t)}{S(t)}. \tag{12}$$

Because the operations of convolution and division do not commute, $R(t)$ is not simply the convolution of $r(t)$ in the sense of Eqs. 2 or 3. Instead, there is a more complicated relationship between $r(t)$ and $R(t)$, as has been pointed out (14, 36), that can cause graphs of $R(t)$ to be somewhat misleading. For example, even if $r(t)$ decays as a single exponential, $R(t)$ can exhibit nonexponential behavior at short times, particularly for values calculated near the initial rising edges of the $S(t)$ and $D(t)$ curves. In addition, the maximum value attained by $R(t)$ at short times is generally $< r(0)$, as noted (14, 36).

In fact, because of convolution it is not possible to have anything but an arbitrary definition for $R(0)$, since the position of time zero on measured decay curves is necessarily arbitrary, it being a time difference between the start and stop pulses. In practice, however, $R(t)$ attains a maximum at a time near the maximum of the instrument function, which is generally taken to be $R(0)$. The differences between $R(t)$ and $r(t)$ naturally diminish as the duration of the instrument function becomes much less than the time scale of interest. The differences have been safely ignored under these circumstances in studies of unrestricted rotational diffusion (30–31) and relatively slow restricted motions (10, 24, 37–39).

However, for some systems $r(t)$ may have a short time component of physical interest. This occurs, for example, when there are two types of processes that can cause depolarization, in general, giving rise to a nonexponential $r(t)$. An example of this is the presence of both a rapid restricted motion of part of a macromolecule and an overall diffusive tumbling of the macromolecule (10, 18, 26). Restricted motions of fluorescent probes in membranes can also produce nonexponential $r(t)$ and have been studied extensively (20, 23, 27, 40–49). There has been considerable theoretical interest in predicting the anisotropy decays that result from such motions (50–52). Torsional motion in DNA has been detected by nonexponential anisotropy decay of an intercalated fluorescent probe (25, 39, 53). Another condition that may cause $r(t)$ to decay nonexponentially is the presence of electronic relaxation processes, which occur even in the absence of molecular motion (54). For example, if two overlapping transitions are excited, $r(t)$ can decay in two phases, an initial rapid decay, which corresponds to attaining a quasi-equilibrium between the excited states, then a slower decay at long times, which corresponds to motion of the molecules.

As the method of time-resolved fluorescence anisotropy is extended to shorter time scales and used to obtain precise information about rapid processes, it is important to be aware of the limitations that are imposed by convolution, systematic errors, and the method of data analysis. In this work we review some of the methods used in the analysis of anisotropy experiments and examine their limitations using both simulated and experimentally obtained data. In addition, we present a new method for determining $r(t)$ by simultaneous fitting of the measured parallel and perpendicular decay functions. This method does not utilize the constructed difference function, nor $R(t)$, and has some advantages over the other methods previously reported, including preserving Poisson statistics, removing redundant parameters from the fitting, and avoiding the propagation of large error in the time region where $r(t)$ approaches zero. In some cases, avoiding error propagation enables this method to detect systematic errors present in the data that would be obscured if the point-by-point difference between the two curves were calculated. We explore the implications of errors in normalization of the experimental curves, fitting over a limited time range, and time shifts in the emission curves relative to the instrument function (generally due to wavelength-department response of the detector). In addition, we demonstrate that the theoretically predicted χ_r^2 of unity can be attained in depolarization experiments.

EXPERIMENTAL

Measurements were made on dilute solutions of two dye molecules. Eosin Y (Eastman Kodak Co., Rochester, NY) was purified by thin layer chromatography on a silica plate (60 F-254; Manufacturing Chemists, Inc, Norwood, OH) using a solvent mixture consisting of 25:15:30 ethanol/chloroform/ethyl acetate, respectively, by volume. Anthracene (Aldrich Chemical Co., Inc., Metuchen, NJ) was used without further purification.

Fluorescence emission curves were measured by time-correlated single photon counting (55). The excitation source for the eosin measurements consisted of an actively mode-locked argon ion laser (CR-6; Coherent Inc., Palo Alto, CA) operating at a repetition rate of 93.54 MHz and a wavelength of 514.5 nm. The ultraviolet (UV) excitation used in the anthracene measurements was generated by synchronous pumping of a rhodamine 6G dye laser (CR-599; Coherent Inc.) with the argon laser, producing visible pulses at 596 nm, which were then frequency doubled by an angle-tuned lithium iodate crystal, yielding 298 nm. The repetition rate of either source was reduced by a low-voltage electrooptic modulator (model 28; Coherent Inc.) driven by a countdown logic circuit synchronized to the mode-locker radio frequency source, selecting pulses at a rate of 91.3 kHz. The contrast ratio between selected and rejected pulses was ~100:1 in the visible and better by at least a factor of five in the UV, where selection was made before harmonic generation. The start signal for the time-to-amplitude converter (457; Ortec Inc., Oak Ridge, TN) was obtained from a constant fraction discriminator (583; Ortec Inc.), which had as input a signal either from a photodiode (BPW 128; AEG-Telefunken Corp., Somerville, NJ) monitoring the pulse train or from the countdown logic. Fluorescence emission detected at right angles to the excitation was detected by a photomultiplier (XP2020; Philips Electronic Instruments, Inc., Mahwah, NJ) after passing through filters that absorbed the scattered excitation light and through a polarizing element (HNP,B plastic; Polaroid Corp., Cambridge, MA) with orientation either parallel, perpendicular, or at the magic angle relative to the polarization of the excitation pulse. The absence of a scattered light contribution in the measured curves was checked by counting for an equivalent time using only the pure solvent. The polarizer was mounted on a rotation stage (RSA-2; Newport Corp., Fountain Valley, CA), which could be positioned to an accuracy of ~0.5°. The photomultiplier output was amplified (600L; ENI Power Systems Inc., Rochester, NY) and sent to a second discriminator, which generated the stop signal. The excitation beam was attenuated so that the ratio of the rates of stop to start pulses was always <2%. The outputs of the time-to-amplitude converter were processed by a multichannel analyzer (1706; Tracor Northern, Middleton, WI) and the accumulated data sent to a VAX 11/780 computer (Digital Equipment Corp., Marlboro, MA) for analysis. The instrument response functions were measured by scattering excitation light with a dilute solution of coffee creamer. In the visible and UV, we obtained 325 and 407 ps, respectively, for the full width at half maximum (FWHM) of the instrument functions.

Because only one trace could be accumulated at a time the parallel and perpendicular curves,collected separately, had to be properly normalized with respect to cumulative excitation intensity. Fluctuations in the intensity of the laser made it impossible to do this accurately by simply collecting curves for equal lengths of time, so the scaling was done with an intensity integrator, which monitored a portion of the excitation beam picked off by a beam splitter. Methods used for scaling by other workers are summarized in the Methods section. The integrator consisted of a photomultiplier (1P28), a voltage-to-frequency converter, and a circuit that counts at a rate proportional to the laser intensity. When a preset value in the counter is attained, a signal is sent to the multichannel analyzer, which stops the experiment. The performance attained by the intensity integrator is discussed in the Results section.

Simulations of fluorescence depolarization experiments were generated to examine the limitations of different methods of data analysis using the following procedure. Experiments were simulated by assuming model forms for $K(t)$ and $r(t)$ of sums of exponentials, then combining them to give $i_\parallel(t)$ and $i_\perp(t)$ using Eqs. 4 and 5. These data were then convoluted with a typical experimental instrument function to obtain the expectation values of the numbers of counts in each channel of the decays. The instrument function used in these simulations had a FWHM of 224 ps because the time base was assumed to be 20 ps per channel for simplicity. Statistical noise is simulated by adding to each channel a pseudorandom number chosen from a Gaussian parent distribution, with mean and variance given by the expectation value for that channel, as is appropriate for counting statistics (32). As with real data, these calculations were performed on the VAX 11/780 computer (Digital Equipment Corp.) of the Department of Chemistry, University of Chicago.

STATISTICAL CRITERIA FOR CURVE FITTING

One of the notable features of photon counting experiments is the statistical nature of curve accumulation. Because in the absence of systematic errors the number of counts in a particular channel follows a Poisson distribution (32), there are some rather strict limitations on the acceptable deviations of the experimental and fitted curves. In our experiments, we used two statistical tests to judge the acceptability of our fits. Values of the statistical parameters for some fits shown are given in Table I; we will briefly discuss those of Fig. 1.

In an experiment where there are no systematic errors present, the properly weighted residuals should have the properties of a set of independent random variables selected from a normal distribution with unit standard deviation. The commonly calculated χ_r^2 then has a precise interpretation beyond that of a number that when minimized gives the best fitting curve; χ_r^2 indicates whether or not systematic errors cause the fitted curve to deviate from the experimental points (57). For example, data shown in Fig. 1 have 493 degrees of freedom, from this we predicted a mean value of χ_r^2 0.999 for χ_r^2, with standard deviation 0.064. The observed value is 1.138, which is 2.185 standard deviations from the predicted mean.

A second important test of the residuals is the runs test, which provides information about the presence of serial correlation among the residuals (57, 58). The number of runs, u, is defined as the number of sequential groupings of residuals with the same sign. Given the number of positive and negative residuals (generally not equal), a probability distribution can be computed for observing a particular number of runs in a given experiment. For example, for the data in Fig. 1, the fitting resulted in 273 positive and 216 negative residuals. The predicted number of runs was 234.0 ± 10.9; we observed 243, which was −0.914 standard deviations from the theoretical mean.

The autocorrelation function of the residuals is often computed and inspected for the appearance of systematic errors. In principle, this inspection tests for the same deviations as the runs test, but more qualitatively. The runs test has the advantage that it gives a quantitative, objective confidence bound.

For both the χ_r^2 and runs tests, we computed the observed normal deviate, Z, given the theoretical mean and standard deviation. This information was routinely generated by our computer programs for each fit. The theoretical likelihood of Z values occurring within a given range can be found easily from tables of the standard normal distribution function (56). For example, it was expected that the absolute value of Z should exceed 2.57 only 1% of the time if the deviation from the mean was purely statistical. Thus, if Z was within a reasonable number of standard deviations from 0, generally taken to be ±3, we concluded that no detectable systematic error is present in the data.

METHODS

There are several approaches discussed in the literature, which deal with overcoming the difficulties in analysis and interpretation of fluorescence depolarization experiments, that have resulted in several methods for

TABLE I
RESULTS OF FITS TO DETERMINE EOSIN $r(t)$

Method	Degrees of freedom	χ_r^2		Runs		$r(0)$	τ_r
		x^* (Z)	$\mu\ddagger$ $\pm\sigma$	x^* (Z)	$\mu\ddagger$ $\pm\sigma$		
							ps
$R(t)$ direct	44	1.45 (+2.18)	0.98 ±0.213	12 (−3.30)	22.9 ±3.3	0.282	308
$D(t)$	497	0.96 (−0.68)	1.00 ±0.063	219 (−2.54)	247 ±11.0	0.359	181
$I_{11}(t)$	495	1.05 (+0.77)	1.00 ±0.064	230 (−1.50)	246 ±11.0	0.450	123
Simultaneous	988	1.11 (+2.44)	1.00 ±0.045	446 (−3.07)	494.1 ±15.7	0.396	157
Polarization spectroscopy	158	—	—	44 (−4.6)	68 ±5.35	NA	157§

*Observed value and standard deviation from predicted mean.
‡Predicted mean value and standard deviation.
§Adjusted for temperature and viscosity from 27°C result.

obtaining $r(t)$. We first briefly review the different reported methods for dealing with the problem of correctly scaling the parallel and perpendicular curves and then discuss several methods that have been used in analysis.

The scaling factor has been previously determined in several ways, which include comparison of parallel and perpendicular count rates over "short" times where the excitation intensity is assumed to be constant (14, 35, 59–60), steady state normalization (12, 13, 17, 38, 40, 44, 61), tail edge matching when $r(t)$ goes to 0 rapidly (11, 31), and front edge matching where $r(0)$ is assumed to be 0.4 (31). Another approach to scaling is to try and make α as close to unity as possible by collecting $I_\parallel$ and $I_\perp$ alternately for short periods, thus accumulating correctly scaled curves. This has been done by rotating the excitation or emission polarizers every few seconds (15, 22, 23, 25, 26, 37, 62–64), or by swapping sample cells to which polarizers of different orientations have been attached (41, 43, 65). One group reported that the dye laser excitation had a stable enough average intensity so that proper scaling was achieved by collecting data for identical times (28).

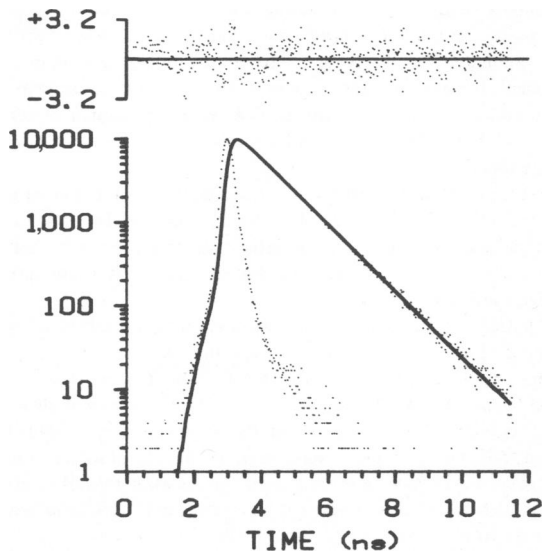

FIGURE 1 Nonlinear least-squares results for fit decay of eosin magic angle fluorescence by single exponential. The rapidly decaying curve is the instrument response function used for the deconvolution. The sample is in water at 20°C. The fit gives $K(t) = \exp(-t/1{,}069\ \text{ps})$. The shift parameter was 53.6 ps. Weighted residuals are shown above the decay. Statistical information for this fit is given and discussed in the Statistical Criteria for Curve Fitting section.

A few groups genuinely collect two curves simultaneously, for example, by using carefully balanced photomultiplier tubes (16), in one case alternating the roles of the two tubes during collection to cancel the effects of differing detection efficiencies (36). Mendelson and co-workers (24) direct the fluorescence into a Wollaston prism which splits the radiation into two orthogonally-polarized beams that diverge by 20°, each detected by a PMT. The information from a time-to-amplitude convertor (TAC) is stored in the appropriate curve by a computer that keeps track of which PMT generated the stop pulse. Wijnaendts Van Resandt and co-workers (29) use a polarizing beam splitter to separate the parallel and perpendicular polarized components of the fluorescence, then focus both beams onto the photomultiplier, one optically delayed by ~12 ns. In this way they accumulate two separated traces at once in a single multichannel analyzer.

Scaling can also be accomplished by monitoring the total fluorescence intensity with a reference PMT (19, 66), which should monitor the fluorescence that passes through a polarizer positioned at the magic angle. We present an additional method of scaling here by monitoring the excitation intensity directly using the intensity integrator described above.

With a few exceptions, most previous methods start by constructing $S(t)$ and $D(t)$. Generally, $S(t)$ is fit to a sum of one or more exponential decays either by least-squares iterative convolution (33) or a combination of truncated moments and iterative convolution (21, 53). One could also use any of the other standard methods for fitting $S(t)$ decays, as reviewed for example by O'Connor et al. (67), including moments, Laplace transforms, exponential series, or Fourier transforms, but these methods have not yet been used in analysis of time-resolved anisotropy experiments. After the parameters for $K(t)$ have been found, $D(t)$ can be fitted to either a single exponential or a sum of exponentials either without any constraints (11, 23, 28, 66) or by varying the $r(t)$ parameters in Eqs. 4, 5, 10, and 11 with the $K(t)$ parameters fixed (12, 23, 27, 35, 40–45, 68). In one case, after $S(t)$ was fitted using a sum of two exponentials, $D(t)$ was fitted using three, with one time constant fixed at the value of the longest time constant found for $K(t)$ (46). One group has used a method where $S(t)$ and $D(t)$ are fit simultaneously by varying both the parameters for $r(t)$ and $K(t)$, although without taking convolution into account (25, 37). Once the fitted parameters for $K(t)$ and $d(t)$ are obtained, $r(t)$ can be

constructed by taking the ratio of these two functions (15, 19, 59, 63–64).

Other methods have concentrated on the function $R(t)$, the point-by-point anisotropy constructed directly from the measured decay curves using Eq. 12. In cases where the width of the instrument function is much less than the relevant decay times, $R(t)$ can be fitted directly to model functions, ignoring the effects of convolution (10, 13, 16, 17, 24, 30, 31, 38, 49, 61). Of course, in this case the fitting range generally begins after the maximum of the $R(t)$ function. Recently, correction factors have been given to account approximately for the effect of convolution on direct fits of $R(t)$ (36).

Convolution of $R(t)$ has been taken into account by some, notably Wahl (14, 34, 69), who has proposed a method for directly fitting $R(t)$. First $S(t)$ is fit, then the $K(t)$ parameters are used with trial $r(t)$ parameters to construct $d(t)$, which is convoluted to generate $D(t)$. Finally, the ratio of the fitting functions is used to generate a trial $R(t)$, which is iteratively compared with the experimental $R(t)$ (14, 34, 61, 69). Wahl accounts for error propagation assuming that the intensities are Poisson distributed to generate variance estimates for the fitted $R(t)$ points, making it possible to use the χ_r^2 test. However, in this method $R(t)$ is fit over a range beginning with its maximum.

Additionally, the novel method of "relative deconvolution" has been used for the case of single exponential $K(t)$ and $r(t)$ in which the instrument response function is not needed in the data analysis (22, 62). This technique uses the fact that the two experimental curves, $I_\parallel(t)$ and $I_\perp(t)$ differ in their mathematical forms in a known way, but are collected under the same instrumental conditions. It is also possible to obtain single exponential $r(t)$ and $K(t)$ parameters by fitting $I_\parallel(t)$ to a double exponential decay (28, 65), but Barkley and co-workers note that even in the absence of systematic errors, the information content in a single curve is probably not sufficient to discriminate between various mechanisms for rotational diffusion (12).

Here we present a new method of anisotropy data analysis by simultaneous fitting of the measured intensity decays. The first step is to determine accurately the excited state fluorescence decay law, $K(t)$, by one or more experiments with the analyzing polarizer oriented at the magic angle from the polarization direction of the excitation pulse. The accumulated curves were individually fit by a standard International Mathematical Software Library nonlinear least-squares program that used the Levenberg-Marquardt algorithm (70, 71) with iterative convolution (33). The usual shift parameter was included to account for the difference between the positions of the instrument function at excitation and emission wavelengths (72).

With particular values for the $K(t)$ parameters at hand, we generated $i_\parallel$ and $i_\perp$ curves given a choice of the form of $r(t)$ and its parameters, using Eqs. 4 and 5. Those generated $i_\parallel$ and $i_\perp$ curves were convoluted with instrument response function using Eqs. 2 and 3, to produce $I_\parallel$ and $I_\perp$, so that two sets of residuals were computed, one for each of the two curves. As in fitting a single curve by iterative convolution, a shift parameter was adjusted during the fit to compensate for a wavelength-dependent delay in the response of the photomultiplier. This shift parameter displaced both curves by equal amounts from the position of the instrument function.

In complete analogy with the usual method of extracting excited state decay times, the results of this fitting procedure were the parameter values of our chosen form of $r(T)$, rather than an independently generated $r(t)$ curve. The appropriateness of the chosen form for $r(t)$ was judged from the quality of the fit.

Since these data points are Poisson distributed, the residuals were weighted assuming $\sigma_i^2 = y_i$. The overall χ^2 (simply the sum of the χ^2's for each curve) was computed and minimized by iteratively varying the parameters in the model $r(t)$. This procedure was simultaneous in that the fitting program minimized the squares of the residuals from both curves at the same time. In this way a single set of parameters was determined, which was the best compromise between the best fitting parameters for either curve. During this fitting process, we fixed the values of the parameters for $K(t)$ at those values determined by the magic angle experiments, but an overall scaling factor for the height of the parallel and perpendicular curves was varied and optimized by the fitting procedure. In experiments where there was a significant long-time portion of the decay curves, where $r(t) \sim 0$ (as in the experimental data presented in this work), the parameters for $K(t)$ could also be varied to determine their best values.

RESULTS

Test of the Intensity Integrator

To test the performance of the integrator and the long term stability of the apparatus, seven decay curves for anthracene in cyclohexane were collected over a period of 4½ h. The set of seven curves contained examples of $I_\parallel(t)$ (2), $I_\perp(t)$ (3), and $I_m(t)$ (2), which should be identical as anthracene rotates rapidly on the time scale of interest. For the 21 combinations of pairs of curves we determined the scaling factor that best matched the two curves using the following procedure. The assumption of counting statistics is that the observed number of counts in channel i is a random variable from a normal distribution with unknown parent mean μ_i and variance μ_i. If two accumulated curves differ only by a scaling factor, this means that all parent values of one curve differ from those of the other by this same multiplicative factor, α, which can be determined by minimizing the quantity χ_r^2, given by

$$\chi_r^2 = \left(\frac{1}{N-1}\right)\sum_{i=1}^{N}[I_1^{(i)} - \alpha I_2^{(i)}]^2/\sigma_i^2, \tag{13}$$

where $I_1^{(i)}$ and $I_2^{(i)}$ are the counts in channel i of curves 1 and 2, respectively. The expected variance of the terms is given by (56)

$$\sigma_i^2 = I_1^{(i)} + I_2^{(i)}. \tag{14}$$

So minimizing Eq. 13 yields

$$\alpha = \frac{\sum_{i=1}^{N} I_1^{(i)} I_2^{(i)}/\sigma_i^2}{\sum_{i=1}^{N}[I_2^{(i)}/\sigma_i]^2}. \tag{15}$$

After α is determined by Eq. 15, the residuals in Eq. 13 are computed and the χ_r^2 and runs statistics are evaluated to check for the presence of systematic error. For the anthracene data, we obtained average values and standard deviations for these tests of $\chi_r^2 = 1.048 \pm 0.098$ ($Z = +0.78 \pm 1.5$) and Z (runs) $= -0.508 \pm 1.095$. The agreement with the predicted $Z = 0 \pm 1$ is good. The average scaling factor determined was 0.9912 ± 0.006, which indicates that the normalization error not compensated for by the integrator was <2%. These experiments also test for and reveal the absence of any polarization bias in the photomultiplier. As a result of these investigations we have confidence in the reproducibility of our data and the stability of the instrument function over the course of a day's data accumulation. Thus statistically based criteria

for judging the goodness of fit of our anisotropy data seem well justified.

Determination of $K(t)$

The first step in analysis of anisotropy experiments is determining the excited state decay law, $K(t)$, which is independent of any molecular reorientations provided that the orientational and electronic degrees of freedom are uncoupled, as is usually the case.

In conjunction with anisotropy measurements, $K(t)$ is commonly found by computing $S(t)$ and fitting it using some standard method, e.g., iterative convolution (33) or moments (73). Alternately, one can obtain $K(t)$ by making a measurement with the analyzing polarizer oriented at the magic angle from the polarization direction of the excitation pulse. This effectively adds the parallel and perpendicular components of the emission to produce a decay curve, $I_m(t)$, which is proportional to $K(t)$.

The magic angle method is routinely used for lifetime measurements, and a best value of the lifetime parameters can be generated by averaging several experiments. In anisotropy experiments, the $K(t)$ parameters are most often determined from $S(t)$ to obtain the fitted value for the overall height of the deconvoluted curves, which is necessary to obtain $r(0)$, and to account for variations in the observed $K(t)$ parameters, which occur from one run to the next. However, the magic angle method has two advantages over fitting $S(t)$. First, because only one curve is required the problems of scaling two decay curves (i.e., accurate determination of α) and of minimizing the systematic variations (e.g., time-origin shifts, long-term changes in response function) between them are avoided. Secondly, in the absence of systematic errors, Poisson statistics apply to the raw data. This latter advantage may seem trivial since error propagation can be applied to the computation of $S(t)$ (14, 43), giving

$$\sigma_s^2 = I_\parallel(t) + 4\,\alpha^2 I_\perp(t). \tag{16}$$

However, if equal time is spent accumulating $I_\parallel$ and $I_\perp$ (i.e., $\alpha = 1$), the error due to counting statistics in $S(t)$ is greater than that for a magic angle decay, which is accumulated for a length of time equal to the sum of times spent collecting $I_\parallel(t)$ and $I_\perp(t)$. The counting errors are equal only if the time collecting parallel and perpendicular curves is partitioned in the ratio 1:2 (i.e., $\alpha = 0.5$).

When $K(t)$ is known to be described by a single exponential decay law, the particular method chosen for finding τ_f is not crucial. But, for nonexponential $K(t)$, the necessity of fitting several parameters increases the sensitivity of the fitting procedures to systematic errors. We now briefly examine the effects of some systematic errors on the $K(t)$ parameters extracted from simulated fluorescence decays.

An incorrect scaling factor can influence lifetimes and amplitudes recovered from fits to $S(t)$. For example, suppose that the correct value of α is unity, but in the analysis we incorrectly assume it has a different value. Then $s(t)$ is given by

$$s(t) = \tfrac{1}{3} K(t)[(1 + 2\alpha) + 2(1 - \alpha)r(t)]. \tag{17}$$

To study this, simulations were done assuming a single exponential $K(t)$ with lifetime of 2 ns and single exponential $r(t) = 0.4 \exp(-t/2\text{ ns})$. Even with gross scaling errors using α incorrect by as much as a factor of two, the decay time recovered was within 5% of the correct decay time. Although the extracted lifetimes were close to the correct value, in some cases the χ_r^2 significantly differed from 1.0, indicating that the systematic error had been detected by the fitting procedure.

Another kind of systematic error examined was a difference in the starting positions (time shifts) of the parallel and perpendicular curves. A number of simulations and fits were done with curves of different heights and time shifts, with the same single exponential r and K parameters used in the previous section. It was found that the χ_r^2 values were consistently higher for pairs of curves that had higher overall heights.

For example, with a shift difference of one channel (20 ps), we obtained the correct decay time for $K(t)$ to within 0.3%, and χ_r^2 values ranged from 0.93–1.02, for curves with parallel heights ranging from 12,000–73,000. However, when the shift error was increased to three channels (60 ps), for curves with parallel heights of 12,000, 24,000, 49,000, and 73,000, we obtained χ_r^2 values of 1.13, 1.58, 2.17, and 2.29, respectively, although the extracted time constants only ranged from 2,011 to 2,013 ps. This is an example of a systematic error which does not significantly effect the extracted time constant for single exponential $K(t)$, although it reveals its presence in a χ_r^2 value that differs from unity.

A demonstration of the results obtained for real systems is given by fitting decays of eosin-Y in water with visible excitation (514.5 nm) and emission (>590 nm). The fit to a magic angle decay with a single exponential at 20°C is shown in Fig. 1. For this fit we obtain $\chi_r^2 = 1.138$ ($Z = +2.18$) and runs $Z = -0.914$. Thus both statistical criteria are statisfied for this fit. We also obtained $I_\parallel(t)$ and $I_\perp(t)$ decays for eosin under the same conditions that the data in Fig. 1 were obtained. These polarized fluorescence data were used for Figs. 2, 3, 4, and 5.

The orientational distribution function of eosin in water at 20°C becomes isotropic within a few nanoseconds after excitation because the molecules are small and their motions are not restricted. Thus, unlike the cases where fluorescent probes are bound to membranes or large proteins, there is no residual anisotropy (r_∞) term. Since $r(t) \sim 0$ for the latter portions of the curves, we corrected $I_\perp$ by a multiplicative factor determined by matching the latter parts of the decays. The scaling algorithm used was that for finding α by Eq. 15, except that only the latter portions of the decays were matched. This corrected small errors in the normalization made by the integrator. In the case of

the eosin data used to generate Fig. 2, 3, 4, and 5, for example, the correction factor was 1.013, i.e., the error in the normalization made by the integrator was 1.3%.

The result of a fit to $S(t)$ for eosin is shown in Fig. 2. The single exponential fluorescence lifetime obtained was 1069.4 ps, in good agreement with the magic angle fit, and the deconvoluted pre-exponential factor is 4.945×10^4. Although the extracted lifetime is correct, neither of the statistical criteria are strictly satisfied: $\chi_r^2 = 1.252$ ($Z = 3.99$) and runs, $Z = -3.28$. This evidently indicates the presence of a slight systematic error that does not effect τ_f. The systematic error is apparently more readily detected in $r(t)$ determinations using simultaneous fitting rather than fitting $D(t)$ or $I_\parallel(t)$; we discuss this topic in the next section.

Determination of $r(t)$

Using both simulated and experimental data, we examined different fitting methods: constructing and fitting $R(t)$ without deconvolution, fitting $D(t)$, fitting $I_\parallel$ only, and simultaneous fitting of $I_\parallel$ and $I_\perp$. Using the same eosin data that appears in Fig. 2, we constructed $R(t)$ with Eq. 12; the resulting function is shown in Fig. 3. As Wahl notes (14), if convolution causes a significant distortion of the measured curves, the interpretation of the anisotropy function generated in this point-by-point fashion is not simple. A confusing feature of such generated functions is that they are clearly nonexponential at short times, even if the true anisotropy is a single exponential. Furthermore, the observed limiting value of $R(0)$ is less than the true initial value (14, 36).

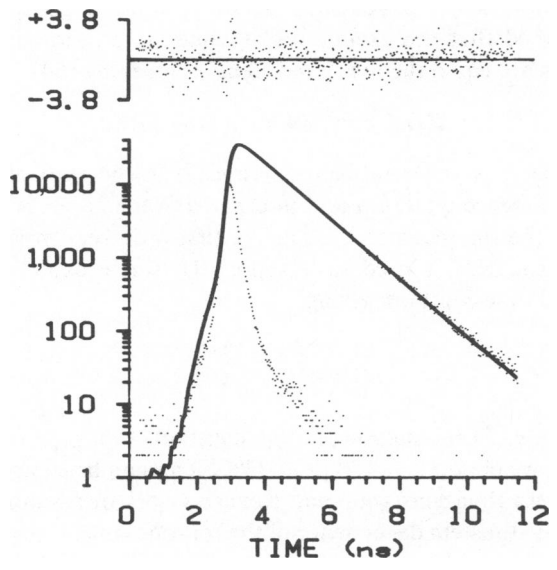

FIGURE 2 Nonlinear least-squares results for fit decay of $S(t)$ calculated from eosin $I_\parallel(t)$ and $I_\perp(t)$ curves. The fit is to a single exponential decay law, $K(t) = 4.94 \times 10^4 \exp(-t/1{,}069 \text{ ps})$. The rapidly decaying curve is the instrument response function. Residuals, weighted by Eq. 16, are shown above the decay. The shift parameter was 32.3 ps. The statistical tests for this fit give $\chi_r^2 = 1.25$ ($Z = +4.0$), $Z_{runs} = -3.3$.

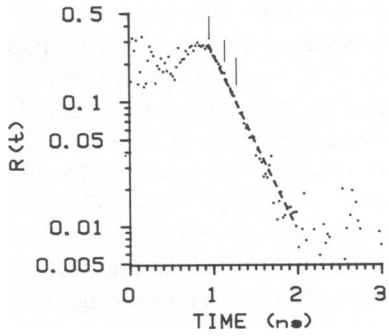

FIGURE 3 Point-by-point anisotropy, $R(t)$, calculated from Eq. 12 using polarized eosin decay curves shown in Fig. 5. The time axis is offset from that in Fig. 5 by 2 ns. Only positive $R(t)$ values are plotted. The vertical dashes indicate, from left to right, the maxima of the instrument function, the parallel, and perpendicular decay curves. The dashed line is a linear least-squares fit that corresponds to $R(t) = 0.282 \exp(-t/308 \text{ ps})$. The correlation coefficient is -0.9935. Data points were weighted according to Eq. 18. The statistical tests for this fit are given in Table I.

Note that the peak of $R(t)$ occurs significantly before the peaks of the measured fluorescence decay functions. The initial part of the $R(t)$ curve is thus determined from the rising edges of the measured curves. This causes doubt on the validity of analyzing $R(t)$ curves only from times greater than the fluorescence emission maxima for rapidly decaying $r(t)$. For $r(t)$, which has time constants much longer than the instrument function width, the initial value of $R(t)$ approaches $r(0)$, as noted by Papenhuijzen and Visser (36).

A linear least-squares fit was done on the plot of $\ln[R(t)]$ vs. t in the region after its maximum. To do this, the estimates of the variances for $R(t)$ in each channel were calculated assuming Poisson statistics apply to $I_\parallel(t)$ and $I_\perp(t)$ and using error propagation (14, 75). In this way and using Eq. 16, we obtain

$$\sigma_R^2 = R^2\left(\frac{\sigma_S^2}{S^2} + \frac{\sigma_D^2}{D^2} - \frac{2\sigma_{SD}^2}{SD}\right), \tag{18}$$

where

$$\sigma_D^2 = I_\parallel + \alpha^2 I_\perp \tag{19}$$

$$\sigma_{SD}^2 = \sigma_S^2 - 2\alpha^2\sigma_D^2. \tag{20}$$

It is interesting that the τ_r extracted from Fig. 3 by this fit in the region after its maximum to a single exponential is 308 ps, which we shall see is almost twice the value obtained by methods that account for convolution. This is so even though the function appears to decay exponentially in this region. Thus, the linearity in the latter part of Fig. 3 is misleading in that convolution has altered the apparent decay constant. Naturally, if τ_r were greater than the instrument function width, the time constant would have been extracted correctly from the slope of a plot of $\ln[R(t)]$ vs. t. But time constants comparable with or less than the instrument function width cannot be extracted from $R(t)$ without taking convolution into account.

The fit to the curve $D(t)$ generated from the same polarized fluorescence data for eosin is shown in Fig. 4. The estimates of the variances given in Eq. 19 are used. It has been noted by Dale and co-workers (43) that use of incorrect variance estimates in such a fit can give rise to errors in the extracted parameters. The fitting criteria obtained are $\chi_r^2 = 0.956$ ($Z = -0.675$), and runs, $Z = 2.538$, which indicates an acceptable fit. The reorientation time, τ_r, is 181 ps. To obtain the $r(0)$, we use $K(0)$ determined from the same data set (Fig. 2), giving $r(0) = 0.359$.

Another method tested with the eosin data was fitting $I_\parallel(t)$ to the convolution of a function of the form

$$i_\parallel(t) = A_1 e^{-t/\tau_1} + A_2 e^{-t/\tau_2} \tag{21}$$

where $\tau_1 > \tau_2$. If we assume that the fluorescence lifetime is longer than the rotational reorientation time, we obtain

$$\tau_r = \left(\frac{1}{\tau_2} - \frac{1}{\tau_1}\right)^{-1} \tag{22}$$

and

$$r(0) = \frac{A_2}{2A_1}. \tag{23}$$

For the fit we obtained $\chi_r^2 = 1.048$ ($Z = 0.77$) and runs, $Z = -1.50$. The decay parameters were $\tau_f = 1{,}062$ ps, $\tau_r = 123$ ps, and $r(0) = 0.450$.

Finally, the result of simultaneous fitting of the eosin data is shown in Fig. 5. The fitting criteria are $\chi_r^2 = 1.109$ ($Z = 2.436$), and runs, $Z = -3.071$. The extracted parameters are $r(0) = 0.396$, $\tau_r = 157.4$ ps.

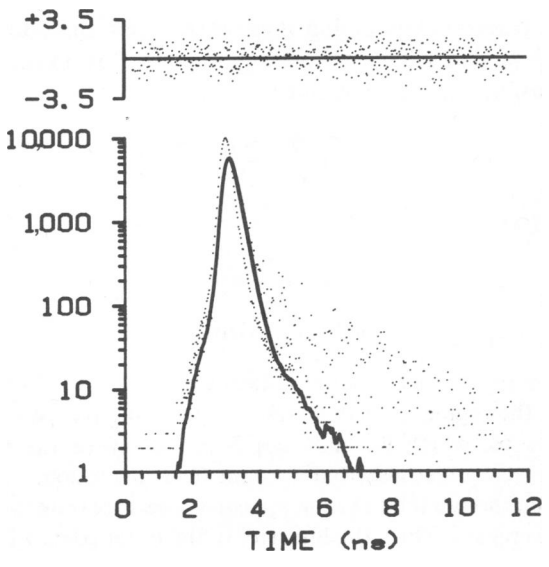

FIGURE 4 Nonlinear least-squares results for fit of decay of $D(t)$ calculated from polarized eosin decay curves. The fit is to a single exponential decay law. Using $K(t)$ parameters from fit in Fig. 2, this fit corresponds to $r(t) = 0.359 \exp(-t/182$ ps). Residuals, weighted according to Eq. 19, are shown above the fit. The shift parameter was 22.1 ps. Statistical tests for this fit are given in Table I. Only positive values of $D(t)$ are shown.

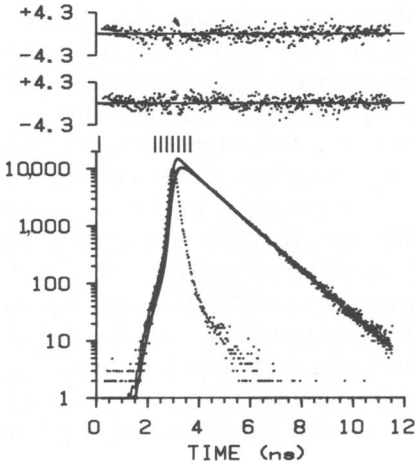

FIGURE 5 Simultaneous fittings results for eosin in water at 20°C. Fitted curves and data points are shown for parallel and perpendicular fluorescence using a fixed excited state decay law, $K(t) = \exp(-t/1{,}070$ ps.). The fitted anisotropy obtained is $r(t) = 0.396 \exp(-t/157$ ps). The shift parameter was 32.2 ps. Residuals, weighted according to Poisson statistics, are shown for both curves, the lower and upper plots are for parallel and perpendicular curves, respectively. Statistical parameters for this fit are given in Table I. The eight vertical dashes above the curves indicate the starting positions of the ranges fit to obtain results in Table II.

To obtain an independent measurement of τ_r, time-resolved polarization spectroscopy (54) was used to measure the ground state rotation time of eosin in water at 27°C by D. Waldeck and M. Chang (personal communication). The anisotropic absorption signal they obtained fit well to a single exponential decay time of 62 ps. If it is assumed that the excited and ground state reorientation times are equal the measured signal is given by (54)

$$I(t) = e^{-2t/\tau_r}[\phi e^{-t/\tau_f} + (1 - \phi)]^2, \tag{24}$$

where τ_r is the rotational lifetime, ϕ is the sum of the fluorescence quantum and internal conversion yields, and τ_f is the fluorescence lifetime. A first-order expansion of this equation is used to interpret the single exponential fitted time constant, giving

$$\frac{1}{\tau_r} = \frac{1}{2}\left(\frac{1}{\tau_m} - \frac{2\phi}{\tau_f}\right), \tag{25}$$

where τ_m is the measured time constant. Using $\phi = 0.26$ (75), we obtain $\tau_r = 128$ ps at 27°C. This can be compared with the time constant obtained in this work by assuming a Stokes-Einstein dependence of the rotation time. Using the ratios of absolute temperatures and viscosities of water at 20 and 27°C, the polarization spectroscopy measurement predicts $\tau_r = 154$ ps at 20°C, which provides a standard for comparison with the fluorescence measurements.

The results of the fluorescence fitting methods are summarized in Table I. Two aspects of the simultaneous

fitting result provide evidence that it gives the best estimate of the $r(t)$ parameters. First, the $r(0)$ value for simultaneous fitting differs from the theoretical limiting value of 0.4 by only 1%. This measurement is also in agreement with the value of 0.40 ± 0.02 obtained by Fleming et al. (31). Second, τ_r obtained by simultaneous fitting is in closest agreement with the polarization spectroscopy value. The agreement with the value obtained by Robbins (180 ± 20 ps) using streak camera techniques is also good (76).

The statistical Z values for the $D(t)$ and $I_\parallel(t)$ fits are somewhat better than those for simultaneous fitting. This indicates that simultaneous fitting is more sensitive to systematic error than these other two methods. Generally, the systematic error is not detected as well by these other methods because the propagated error due to counting statistics serves to mask the presence of systematic errors. Because the simultaneous fitting is made directly on the measured curves rather than on curves constructed from the data, the Poisson statistics that apply to the number of counts recorded in each channel are preserved. Even if the instrument function is so narrow that convolution does not effect the decay curves, construction of the function $R(t)$ introduces scatter into the data. Although the propagation of errors made in this way can be calculated and has been treated properly by Wahl for $R(t)$ (14), such manipulations always increase the scatter in the resultant data and tend to mask systematic errors that may be present.

Also, because $D(t)$ is the convolution of $r(t)$ $K(t)$, the accuracy in $r(0)$ extracted from fitting $D(t)$ will always be limited by the accuracy of the value of $K(0)$ extracted from the corresponding fit to $S(t)$. In the simultaneous fitting method, a parameter for the overall height is also fit, but it is essentially the ratio of heights of the two curves that determine $r(0)$ rather than the overall height.

Because the rising edges of the fluorescence curve apparently contain important information about the short time behavior of $r(t)$, this might cast doubt on the validity of results obtained when the rising edge of the curve (or curves) is not fit, as is often the case when the instrument function shape is sensitive to emission wavelength (72). We have investigated this point for the data presented here by varying the range over which the data are fit in the simultaneous and difference fitting procedures.

Table II shows the results of this investigation for the eosin data. For this data set, the peaks of the instrument function, and parallel and perpendicular decay curves occur at channel numbers 130, 138, and 144, respectively. If the fitting is begun after the peak of $I_\parallel$ (channel 138), the $r(0)$ and τ_r values extracted by either method are significantly in error. Not surprisingly, if the fit is begun after the $I_\parallel$ and $I_\perp$ curves have almost merged (e.g., channel 160), nonsensical results are obtained for the $r(0)$ and α values even though the χ_r^2 is good.

Another test for the influence of fitting ranges was made by simulating decay curves assuming that $K(t)$ was a single exponential decay with a lifetime of 1.0 ns, and the

TABLE II
FITTED PARAMETERS OBTAINED FOR EOSIN DATA AS FUNCTION OF FITTING RANGE

Range (channel number)	Simultaneous fit			$D(t)$ fit		
	χ_r^2	$r(0)$	τ_r	χ_r^2	$r(0)$	τ_r
1:500	1.11	0.396	157	0.96	0.358	181
100:500	1.16	0.395	157	1.00	0.358	181
110:500	1.17	0.395	158	1.01	0.358	181
120:500	1.17	0.394	158	1.02	0.357	182
130:500	1.08	0.377	167	0.95	0.333	207
140:500	1.01	0.293	205	0.93	0.509	246
150:500	1.01	0.228	247	0.94	0.850	240
160:500	1.00	2.89	71	0.95	1.179	206

anisotropy was heterogeneous, with $r(t) = 0.30\exp(-t/5$ ns$) + 0.10\exp(-t/100$ ps$)$. If the data were analyzed assuming a single exponential $r(t)$ fitting over the entire range for simultaneous fitting, we obtained $\chi_r^2 = 1.52$ ($Z = -4.0$), $r(0) = 0.326$, $\tau_r = 3.94$ ns, while for fits to $D(t)$ we obtained $\chi_r^2 = 1.32$ ($Z = -1.8$), $r(0) = 0.320$, $\tau_r = 4.28$ ns. Thus, both methods detect the presence of systematic error, namely an incorrect functional form, although the simultaneous methods results are somewhat more sensitive to the error as evidenced by the larger χ_r^2 and $|Z|$ value. When the decays were fit over a time range that started after the peak of the fluorescence decay functions, a single exponential $r(t)$ with a lifetime of ~5 ns gave acceptable statistical criteria, indicating that it may be necessary to fit at least part of the rising edges of the curves to obtain reliable short components of a nonexponential $r(t)$. Simultaneous fitting gave better results than $D(t)$ fitting in the sense that as the lower time limit of the fit was decreased to include the rising edges of the curves, the statistical criteria for the single exponential fits for simultaneous fitting began to indicate the presence of systematic error before the critera for $D(t)$ fits.

Additional simulations were done to test the response of the methods to a different kind of systematic error. Before convolution, the fluorescence decay functions were multiplied by a factor

$$x(t) = \left[1 + \epsilon\sin\left(\frac{t+\phi}{\tau}\right)\right]. \tag{26}$$

For the simulations, we chose a single exponential $K(t)$ with a lifetime of 1 ns and $r(t) = 0.4\exp(-t/100$ ps$)$. The period of the sinusoidal noise was 1 ns, and the relative amplitude ϵ was 0.05. When the parallel and perpendicular curves were generated with the noise 180° out-of-phase (i.e., $\phi_\parallel - \phi_\perp = 500$ ps), both simultaneous fitting and $D(t)$ fitting detected the presence of systematic error, as indicated by $\overline{\chi}_r^2 = 2.2$, and $\overline{\chi}_r^2 = 2.5$, respectively. However, when the phases of the noise were the same in both curves, the simultaneous fits gave $\overline{\chi}_r^2 = 1.9$, while $D(t)$ fits gave $\overline{\chi}_r^2 = 0.9$. In the latter case, the $D(t)$ fit failed to detect the systematic error. Averaging over all cases, we obtained for

the percent error in the extracted $r(0)$ and τ_r, 8 and 15%, respectively, for $D(t)$ fitting and 3 and 17%, respectively, for simultaneous fitting.

DISCUSSION

We have reviewed the different methods used to analyze time-resolved fluorescence anisotropy data and explored the effects of some systematic errors on the extracted parameters. It has been demonstrated that to obtain reliable information about rapid anisotropy decays, convolution must be taken into account, and the rising edges of the fluorescence curves should be included in the analysis. The results in Table II demonstrate that even if the fits are begun from the maximum of the fluorescence emission curves, it is possible to introduce significant error in the extracted anisotropy parameters. Simulations of heterogeneous anisotropy decays showed that it is possible to overlook a short component in the anisotropy if the fitting range does not include enough of the beginning portions of the decays, although the simultaneous fitting method needs less of a range to detect the presence of a short component.

The commonly used method of fitting $D(t)$ can give accurate results, but because of the manipulation of the data in constructing the difference function, there is a tendency to mask systematic errors that may be present. Thus, in precise work where the anisotropy decay law is nonexponential, it is possible that a fit to $D(t)$ may appear to be correct even though the model function is incorrect. Because the simultaneous fitting method acts on the raw data rather than constructs of it, it is more sensitive to systematic errors and has been shown in some cases to detect errors when other methods cannot.

Knutson and co-workers (77) recently described a method for simultaneous analysis of sets of time-resolved fluorescence decays. The method is applied to the case where there are two decay components with known identical decay times in each curve, but differing ratios of pre-exponential factors. They demonstrate that the global method gives superior results to fitting the individual curves separately, because it takes into account the relations that exist between the individual decay curves. Our method of simultaneous fitting similarly takes into account the relationship between parallel and perpendicular decay curves, and analogously produces results superior to those obtained when fitting the parallel curve only, for example.

Our method differs from the method of Knutson et al. (77) in that we fit only two curves simultaneously while they can fit several. However, we note that several polarized fluorescence curves could be accumulated at various settings of the analyzing polarizer between the parallel and perpendicular directions generating a set of curves with known relationships, so that there is the possibility of using the global method to analyze anisotropy experiments.

The case of single exponential $r(t)$ and $K(t)$ is the simplest experimentally. Extra parameters introduced in the fitting procedure from nonexponential $r(t)$ and/or $K(t)$ place a greater constraint on the care with which the fitting must be done. In addition, for experiments in the UV (e.g., on tryptophan), there is the difficulty of a greater wavelength dependence of the photomultiplier response than in the visible region. We will address these issues in detail in a future publication.

We thank Mary Chang and David Waldeck for providing the anisotropic absorption result and Dr. Jim Longworth for his comments on an earlier draft of this paper.

This work was supported by grants from the National Institutes of Health (PHS-5 ROI-GM 27825) and Standard Oil of Ohio (SOHIO).

Received for publication 5 April 1983 and in final form 20 January 1984.

REFERENCES

1. Badea, M. G., and L. Brand. 1979. Time-resolved fluorescence measurements. *Methods Enzymol.* 61:378–425.
2. Wahl, Ph. 1975. Decay of fluorescence anisotropy. *In* Biochemical Fluorescence: Concepts. R. F. Chen and H. Edelhoch, editors. Marcel Dekker, Inc., New York. 1:1–41.
3. Isenberg, I. 1975. Time decay fluorimetry by photon counting. *In* Biochemical Fluorescence: Concepts. Marcel Dekker, Inc., New York. 1:43–77.
4. Yguerabide, J. 1972. Nanosecond fluorescence spectroscopy of macromolecules. *Methods Enzymol.* 26C:498–577.
5. Rigler, R., and M. Ehrenberg. 1973. Molecular interactions and structure as analyzed by fluoresence relaxation spectroscopy. *Q. Rev. Biophys.* 6:139–199.
6. T. Tao. 1969. Time-dependent fluorescence depolarization and Brownian rotational diffusion coefficients of macromolecules. *Biopolymers.* 8:609–632.
7. Belford, G. G., R. L. Belford, and G. Weber. 1972. Dynamics of fluorescence polarization in macromolecules. *Proc. Natl. Acad. Sci. USA.* 69:1392–1393.
8. Chuang, T. J., and K. B. Eisenthal. 1972. Theory of fluorescence depolarization by aniostropic rotational diffusion. *J. Chem. Phys.* 57:5094–5097.
9. Ehrenberg, M., and R. Rigler. 1972. Polarized fluorescence and rotational Brownian motion. *Chem. Phys. Lett.* 14:539–544.
10. Tran, C. D., G. S. Beddard, and A. D. Osborne. 1982. Secondary structure and dynamics of glucagon in solution. *Biochim. Biophys. Acta.* 709:256–264.
11. Rice, S. A., and G. A. Kenney-Wallace. 1980. Time-resolved fluorescence depolarization studies of rotational relaxation in viscous media. *Chem. Phys.* 47:161–170.
12. Barkley, M. D., A. A. Kowalczyk, and L. Brand. 1981. Fluorescence decay studies of anisotropic rotations of small molecules. *J. Chem. Phys.* 75:3581–3593.
13. Georghiou, S., M. Thompson, and A. K. Mukhopadhyay. 1981. Melittin-phospholipid interaction evidence for melittin aggregation. *Biochim. Biophys. Acta.* 642:429–432.
14. Ph. Wahl. 1979. Analysis of fluorescence anisotropy decays by a least-squares method. *Biophys. Chem.* 10:91–104.
15. Hanson, D. C., J. Yguerabide, and V. N. Schumaker. 1981. Segmental flexibility of immunoglobulin G antibody molecules in solution: A new interpretation. *Biochemistry.* 20:6852.
16. Harvey, S. C., and H. C. Cheung. 1977. Fluorescence depolarization studies on the flexibility of myosin rod. *Biochemistry.* 16:5181–5187.
17. Holowka, D. A., and R. E. Cathou. 1976. Conformation of immunoglobulin m. II. nanosecond fluorescence depolarization analysis of segmental flexibility in anti-ε-l-dimethylamino-5-napthalenesulfo-

nyl-L-lysine anti-immunoglobulin from horse, pig and shark. *Biochemistry.* 15:3379–3390.
18. Chang, M. C., A. J. Cross, and G. R. Fleming. 1983. Internal dynamics and overall motion of lysozyme studied by fluorescence depolarization of the eosin lysozyme complex. *J. Biomolec. Struct. Dynam.* 1:299–318.
19. Zinsli, P. E. 1979. Inhomogeneous interior of aerosol OT microemulsions probed by fluorescence and polarization decay. *J. Phys. Chem.* 83:3223–3231.
20. Wolber, P. K., and B. S. Hudson. 1982. Bilayer acyl chain dynamics and lipid-protein interaction. *Biophys. J.* 37:253–260.
21. Valeur, B., and J. Moirez. 1973. Analyse des courbes de décroissance multiexponentielles par la méthode des fonctions modulatrices. Application a la fluorescence. *J. Chim. Phys.* 70:500–506.
22. Ricka, J., K. Amsler, and Th. Binkert. 1983. Flexibility of a labeled polymer chain: time-resolved fluorescence depolarization measurements and their interpretation by a hinged-dumbell model. *Biopolymers.* 22:1301–1318.
23. Martin, C. E., and D. C. Foyt. 1978. Rotational relaxation of 1,6-diphenyl-hexatriene in membrane lipids of cells acclimated to high and low growth temperatures. *Biochemistry.* 17:3587–3591.
24. Mendelson, R. A., M. F. Morales, and J. Botts. 1973. Segmental flexibility of the S-1 moiety of myosin. *Biochemistry.* 12:2250–2255.
25. Millar, D. P., R. J. Robbins, and A. H. Zewail. 1980. Direct observation of the torsional dynamics of DNA and RNA by picosecond spectroscopy. *Proc. Natl. Acad. Sci. USA.* 77:5593–5597.
26. Munro, I., I. Pecht, and L. Stryer. 1979. Subnanosecond motions of tryptophan residues in proteins. *Proc. Natl. Acad. Sci. USA.* 76:55–60.
27. Kinoshita, K., Jr., R. Kataoka, Y. Kimura, O. Gotoh, and A. Ikegami. 1981. Dynamic structure of biological membranes as probed by 1,6-diphenyl-1,3,5-hexatriene: A nanosecond fluorescence depolarization study. *Biochemistry.* 20:4270–4277.
28. Spears, K. G., and L. E. Cramer. 1978. Rotational diffusion in aprotic and protic solvents. *Chem. Phys.* 30:1–8.
29. Wijnaendts Van Resandt, R. W., and L. De Maeyer. 1981. Picosecond rotational diffusion by differential single-photon fluorescence spectroscopy. *Chem. Phys. Lett.* 78:219–223.
30. Beddard, G. S., T. Doust, and J. Hudales. 1981. Structural features in ethanol-water mixtures revealed by picosecond fluorescence anisotropy. *Nature (Lond.).* 294:145–146.
31. Fleming, G. R., J. M. Morris, and G. W. Robinson. 1976. Direct observation of rotational diffusion by picosecond spectroscopy. *Chem. Phys.* 17:91–100.
32. Harris, C. M., and B. K. Selinger. 1979. Single-photon decay spectroscopy. II. The pile-up problem. *Aust. J. Chem.* 32:2111–2129.
33. Grinwald, A., and I. Z. Steinberg. 1974. On the analysis of fluorescence decay kinetics by the method of least-squares. *Anal. Biochem.* 59:583–598.
34. Ph. Wahl. 1977. Statistical accuracy of rotational correlation times determined by the photocounting pulse fluorimetry. *Chem. Phys.* 22:245–256.
35. Ross, J. B. A., C. J. Schmidt, and L. Brand. 1981. Time-resolved fluorescence of the two tryptophans in horse liver alcohol dehydrogenase. *Biochemistry.* 20:4369–4377.
36. Papenhuijzen, J., and A. J. W. G. Visser. 1983. Simulation of convoluted and exact emission anisotropy decay profiles. *Biophys. Chem.* 17:57–65.
37. Millar, D. P., R. J. Robbins, and A. H. Zewail. 1982. Torsion and bending of nucleic acids studied by subnanosecond time-resolved fluorescence depolarization of intercalated dyes. *J. Chem. Phys.* 76:2080–2094.
38. T. Tao. 1978. Nanosecond fluorescence depolarization studies on actin labeled with 1,5-iaedans and dansyl chloride. *FEBS (Fed. Eur. Biochem. Soc.) Lett.* 93:146–150.
39. Askikawa, I., K. Kinosita, Jr., A. Ikegami, Y. Nishimura, M. Tsuboi, K. Wantanabe, and K. Iso. 1983. Dynamics of DNA in chromatin and DNA binding mode to core protein. *J. Biochem. (Tokyo).* 93: 665–668.
40. Kawato, K., K. Kinoshita, Jr., and A. Ikegami. 1977. Dynamic structure of lipid bilayers studied by nanosecond fluorescence techniques. *Biochemistry.* 16:2319–2324.
41. Chen, L. A., R. E. Dale, S. Roth, and L. Brand. 1977. Nanosecond time-dependent fluorescence depolarization of diphenylheactriene in dimyristoyllecithin vesicles and the determination of "microviscosity." *J. Biol. Chem.* 252:2163–2169.
42. Badea, M. G., R. P. DeToma, and L. Brand. 1978. Nanosecond relaxation processes in liposomes. *Biophys. J.* 24:197–212.
43. Dale, R. E., L. A. Chen, and L. Brand. 1977. Rotational relaxation of the "microviscosity" probe diphenylhexatriene in paraffin oil and egg lecithin vesicles. *J. Biol. Chem.* 252:7500–7510.
44. Kawato, S., K. Kinoshita, Jr., and A. Ikegami. 1978. Effect of cholestrol on the molecular motion in the hydrocarbon region of lecithin bilayers studied by nanosecond fluorescence techniques. *Biochemistry.* 17:5026–5031.
45. Wahl, Ph., M. Kasai, and J.-P. Changeux. 1977. A study on the motions of proteins in excitable membrane fragments by nanosecond fluorescence polarization spectroscopy. *Eur. J. Biochem.* 18:332–341.
46. Wolber, P. K., and B. S. Hudson. 1981. Fluorescence lifetime and time-resolved polarization anisotropy studies of acyl chain order and dynamics in lipid bilayers. *Biochemistry.* 20:2800–2810.
47. Jonas, A., J.-P. Privat, and Ph. Wahl. 1983. Time-dependent fluorescence intensity and depolarization of diphenylhexatriene in micellar complexes of apolipoprotein C-I and dimyristoylglycerophosphocholine. *Eur. J. Biochem.* 133:173–177.
48. Veatch, W. R., and L. Stryer. 1977. Effect of cholesterol on the rotational mobility of diphenylhexatrienes in liposomes. A nanosecond fluorescence anisotropy study. *J. Mol. Biol.* 177:1109–1113.
49. Visser, A. J. W. G. 1982. Limited rotational motion of amphiphilic flavins in diapacmitoylphosphatidylcholine vesicles. *Biochim. Biophys. Acta.* 692:244–251.
50. Kinoshita, K. Jr., S. Kawato, and A. Ikegami. 1977. A theory of fluorescence polarization decay in membranes. *Biophys. J.* 20:289–305.
51. Lipari, G. and A. Szabo. 1980. Effect of librational motion in fluorescence depolarization and nuclear magnetic resonance relaxation in macromolecules and membranes. *Biophys. J.* 30:489–506.
52. Jahnig, F. 1979. Structural order of lipids and proteins in membranes: evaluation of fluorescence anisotropy data. *Proc. Natl. Acad. Sci. USA.* 76:6361–6365.
53. Genest, D., and Ph. Wahl. 1978. Fluorescence anisotropy decay due to rotational Brownian motion of ethidium intercalated in double strand DNA. *Biochim. Biophys. Acta.* 521:502–509.
54. Cross, A. J., D. H. Waldeck, and G. R. Fleming. 1983. Time resolved polarization spectroscopy: level kinetics and rotational diffusion. *J. Chem. Phys.* 78:6455–6467.
55. Robbins, R. J., G. R. Fleming, G. S. Beddard, G. W. Robinson, P. J. Thistlethwaite, and G. J. Woolfe. 1980. Photophysics of aqueous tryptophan: pH and temperature effects. *J. Am. Chem. Soc.* 102:6271–6279.
56. Hoel, P. G., S. C. Port, and C. J. Stone. 1971. Introduction to Probability Theory. Houghton Mifflin Co., Boston. 258.
57. Draper, N., and H. Smith. 1981. Applied Regression Analysis. John Wiley and Sons, New York. 153.
58. Swed, F. S., and C. Eisenhart. 1943. Tables for testing randomness of grouping in a sequence of alternatives. *Ann. Math. Stat.* 14:66–87.

59. Snare, M. J., K. L. Tan, and F. E. Treloar. 1982. Fluorescence studies of solubilization and dye binding in hypercoiled poly-(methacrylic acid). A connected cluster model. *J. Macromol. Sci. Chem.* 17:189–201.
60. Ikkai, T., Ph. Wahl, and J.-C. Auchet. 1979. Anisotropy decay of labelled actin. *Eur. J. Biochem.* 93:397–408.
61. Lovejoy, C., D. Holowka, and R. E. Cathou. 1977. Nanosecond fluorescence spectroscopy of pyrenebutyrate-anti-pyrene antibody complexes. *Biochemistry.* 16:3668–3672.
62. Ricka, J. 1981. Evaluation of nanosecond pulse-fluorometry measurements. No need for the excitation function. *Rev. Sci. Instrum.* 52:196–199.
63. Wahl, Ph. 1969. Mesure de la decroissance de la fluorescence polarisée de la fluorescence polarisee de la γ-globuline-1-sulfonyl-5-dimethylamino-napthalene. *Biochim. Biophys. Acta.* 175:55–64.
64. Valeur, B., and L. Monnerie. 1976. Dynamics of macromolecular chains. III. Time-dependent fluorescence polarization studies of local motions of polystyrene in solution. *J. Polym. Sci. Part A-2.* 14:11–27.
65. Ross, J. B. A., K. Rousslang, and L. Brand. 1981. Time-resolved fluorescence and anisotropy decay of the tryptophan in andrenocorticotropin (1-24). *Biochemistry.* 20:4361–4377.
66. Tschanz, H. P., and Th. Binkert. 1976. The precise measurement of the fluorescence polarization anisotropy by single-photon counting. *J. Phys. E. Sci. Instrum.* 9:1131–1136.
67. O'Connor, D. V., W. R. Ware, and J. C. Andre. 1979. Deconvolution of fluorescence decay curves. A critical comparison of techniques. *J. Phys. Chem.* 83:1333–1343.
68. Thomas, J. C., S. A. Allison, C. J. Appellof, and J. M. Schurr. 1980. Torsion dynamics and depolarization of fluorescence of linear macromolecules. II. Fluorescence polarization anisotropy measurements on a clean viral ϕ29 DNA. *Biophys. Chem.* 12:177–188.
69. Tawada, K., Ph. Wahl, and J.-C. Auchet. 1978. Study of actin and its interactions with heavy meromyosin and the regulatory proteins by the pulse fluorimetry in polarized light of a fluorescent probe attached to an actin cysteine. *Eur. J. Biochem.* 88:411–419.
70. Levenberg, K. 1944. A method of the solution of certain non-linear problems in least squares. *Quart. Appl. Math.* 2:164–168.
71. Marquardt, D. W. 1963. An algorithm for least-squares estimation of nonlinear parameters. *J. Soc. Ind. Appl. Math.* 11:431–441.
72. Wahl, Ph., J. C. Auchet, and B. Donzel. 1974. The wavelength dependence of the response of a pulse fluorometer using the single photoelectron counting method. *Rev. Sci. Instrum.* 45:28–32.
73. Isenberg, I., R. D. Dyson, and R. Hanson. 1973. Studies on the analysis of fluorescence decays data by the method of moments. *Biophys. J.* 13:1090–1115.
74. Bevington, P. R. 1969. Data Reduction and Error Analysis for the Physical Sciences. McGraw-Hill, Inc., New York. 336.
75. Fleming, G. R., A. W. E. Knight, J. M. Morris, R. J. S. Morrison, and G. W. Robinson. 1977. Picosecond fluorescence studies of xanthene dyes. *J. Am. Chem. Soc.* 99:4306–4311.
76. Robbins, R. J. 1980. Picosecond fluorescence spectroscopy. Ph.D. Thesis, University of Melbourne, Melbourne, Australia. 521.
77. Knutson, J. R., J. M. Beechem, and L. Brand. 1983. Simultaneous analysis of multiple fluorescence decay curves: a global approach. *Chem. Phys. Lett.* 102:501–507.